Energetic outer zone electron loss timescales during low geomagnetic activity

Nigel P. Meredith,[1] Richard B. Horne,[1] Sarah A. Glauert,[1] Richard M. Thorne,[2] Danny Summers,[3,4] Jay M. Albert,[5] and Roger R. Anderson[6]

Received 3 November 2005; revised 1 February 2006; accepted 9 February 2006; published 27 May 2006.

[1] Following enhanced magnetic activity the fluxes of energetic electrons in the Earth's outer radiation belt gradually decay to quiet-time levels. We use CRRES observations to estimate the energetic electron loss timescales and to identify the principal loss mechanisms. Gradual loss of energetic electrons in the region $3.0 \leq L \leq 5.0$ occurs during quiet periods ($Kp < 3^-$) following enhanced magnetic activity on timescales ranging from 1.5 to 3.5 days for 214 keV electrons to 5.5 to 6.5 days for 1.09 MeV electrons. The intervals of decay are associated with large average values of the ratio f_{pe}/f_{ce} (>7), indicating that the decay takes place in the plasmasphere. We compute loss timescales for pitch-angle scattering by plasmaspheric hiss using the PADIE code with wave properties based on CRRES observations. The resulting timescales suggest that pitch angle scattering by plasmaspheric hiss propagating at small or intermediate wave normal angles is responsible for electron loss over a wide range of energies and L shells. The region where hiss dominates loss is energy-dependent, ranging from $3.5 \leq L \leq 5.0$ at 214 keV to $3.0 \leq L \leq 4.0$ at 1.09 MeV. Plasmaspheric hiss at large wave normal angles does not contribute significantly to the loss rates. At $E = 1.09$ MeV the loss timescales are overestimated by a factor of $\sim$5 for $4.5 \leq L \leq 5.0$. We suggest that resonant wave-particle interactions with EMIC waves, which become important at MeV energies for larger L ($L > \sim 4.5$), may play a significant role in this region.

Citation: Meredith, N. P., R. B. Horne, S. A. Glauert, R. M. Thorne, D. Summers, J. M. Albert, and R. R. Anderson (2006), Energetic outer zone electron loss timescales during low geomagnetic activity, *J. Geophys. Res.*, *111*, A05212, doi:10.1029/2005JA011516.

1. Introduction

[2] Energetic electrons ($E > 100$ keV) in the Earth's radiation belts are generally confined to two distinct regions. The inner radiation belt lies in the range $1.2 < L < 2.5$ and exhibits long-term stability. In contrast, the outer radiation belt, which lies in the range $3 < L < 7$, is highly dynamic, particularly during enhanced magnetic activity [e.g., *Paulikas and Blake*, 1979; *Baker et al.*, 1986, 1994, 1997; *Li et al.*, 1997; *Reeves et al.*, 1998]. This variability is caused by an imbalance between acceleration and loss processes both of which tend to be enhanced during magnetically disturbed periods [e.g., *Summers et al.*, 2004]. Understanding this variability is important since enhanced fluxes of relativistic electrons ($E > 1$ MeV) damage satellites in Earth orbit and pose a risk to humans in space. Indeed, enhanced fluxes of relativistic electrons have been associated with a number of spacecraft anomalies and even failures [*Baker et al.*, 1998a; *Baker*, 2001]. Consequently, predicting their appearance has become one of the outstanding challenges of magnetospheric physics. Furthermore, energetic electrons can penetrate to low altitudes where they affect the ionization, conductivity, and chemistry of the stratosphere and mesosphere [e.g., *Thorne*, 1980; *Lastovicka*, 1996; *Callis et al.*, 1998], thereby providing an important coupling mechanism between the magnetosphere and the middle atmosphere.

[3] Electrons with energies up to a few hundred keV are injected into the inner magnetosphere during storms and substorms. Injection of electrons in the energy range 10–100 keV into the outer zone leads to the excitation of intense whistler mode chorus waves outside the plasmasphere on the dawnside of the magnetosphere [e.g., *Tsurutani and Smith*, 1977; *Meredith et al.*, 2001, 2003a]. At higher energies, injected electrons with energies in the range 100–300 keV form a seed population of electrons [e.g., *Baker et al.*, 1998b; *Obara et al.*, 2000] which may subsequently be accelerated to relativistic energies by processes acting within the magnetosphere itself [*Li et al.*, 1997]. While several acceleration mechanisms have been

[1]British Antarctic Survey, Natural Environment Research Council, Cambridge, UK.
[2]Department of Atmospheric and Oceanic Sciences, University of California, Los Angeles, Los Angeles, California, USA.
[3]Department of Mathematics and Statistics, Memorial University of Newfoundland, St John's, Newfoundland, Canada.
[4]Also at School of Physics, University of KwaZulu-Natal, Durban, South Africa.
[5]Space Vehicles Directorate, Air Force Research Laboratory, Hanscom Air Force Base, Massachusetts, USA.
[6]Department of Physics and Astronomy, University of Iowa, Iowa City, Iowa, USA.

0148-0227/06/2005JA011516

proposed (see the reviews by *Li and Temerin* [2001], *Horne* [2002], and *Friedel et al.* [2002]), recent experimental and modelling work suggests that the acceleration is caused by a combination of enhanced inward radial diffusion driven by ULF waves [e.g., *Elkington et al.*, 1999; *Liu et al.*, 1999; *Hudson et al.*, 2000] and local, chorus-driven acceleration outside the plasmapause [e.g., *O'Brien et al.*, 2003; *Horne et al.*, 2006; *Summers et al.*, 2005; *Varotsou et al.*, 2005]. However, during quiet conditions following enhanced magnetic activity, the acceleration processes are ineffective and the energetic electrons gradually decay to their quiet time values. In order to understand radiation belt variability and develop more realistic physical models, it is essential to understand and quantify the decay processes. The periods of gradual decay provide a unique possibility to isolate the loss processes acting during these intervals and to determine the decay lifetimes.

[4] There are several loss mechanisms that operate during quiet time decay. Coulomb collisions with atmospheric constituents are important in the inner zone and are the dominant loss mechanism closest to the Earth, while resonant interactions with plasma waves become increasingly important farther out. The region where Coulomb collisions dominate is energy-dependent, ranging from $L < 2.2$ for 100 keV electrons to $L < 1.4$ for 1.5 MeV electrons [*Abel and Thorne*, 1998]. Ground-based VLF transmitters, used for communications with submarines, leak out of the atmosphere at night and propagate in the inner magnetosphere in the whistler mode. These waves are most important just outside the region dominated by Coulomb collisions. Using average wave characteristics as input to their model, *Abel and Thorne* [1998] showed that pitch-angle scattering by VLF transmitters is likely to be the most effective loss mechanism for 100 keV electrons in the region from $2.2 < L < 2.8$ and for 1.5 MeV electrons in the region $1.4 < L < 2.2$. Lightning-generated whistlers are most effective just outside the region dominated by VLF transmitters, being most effective from $2.8 < L < 4.4$ for 100 keV electrons and from $2.2 < L < 2.6$ for 1.5 MeV electrons [*Abel and Thorne*, 1998]. Farther out, but remaining inside the plasmapause, resonant interactions with both plasmaspheric hiss and electromagnetic ion cyclotron (EMIC) waves are believed to dominate [*Thorne et al.*, 1973; *Lyons et al.*, 1972; *Albert*, 1994; *Summers and Thorne*, 2003; *Summers*, 2005]. Outside of the plasmapause, whistler mode chorus waves can contribute effectively to the loss of energetic electrons [*Horne and Thorne*, 2003; *O'Brien et al.*, 2004; *Thorne et al.*, 2005a; *Summers et al.*, 2005].

[5] The studies described above have identified loss timescales in various regions but have been limited in the coverage of energies and L shells. Here we provide a more extensive survey using the CRRES data set. The objectives are to determine experimentally the loss timescales for energetic electrons over a wide range of energies and L shells, to determine the conditions associated with loss, and to identify the principal loss mechanisms.

2. Instrumentation

[6] The Combined Release and Radiation Effects Satellite (CRRES) is particularly well-suited to studies of wave-particle interactions in the radiation belts both because of its orbit and sophisticated suite of wave and particle instruments [*Johnson and Kierein*, 1992]. The spacecraft was launched on 25 July 1990 and operated in a highly elliptical geosynchronous transfer orbit with a perigee of 305 km, an apogee of 35,768 km, and an inclination of 18°. The orbital period was approximately 10 hours, and the initial apogee was at a magnetic local time (MLT) of 0800 MLT. The magnetic local time of apogee decreased at a rate of approximately 1.3 hours per month until the satellite failed on 11 October 1991, when its apogee was at about 1400 MLT. The satellite swept through the heart of the radiation belts on average approximately 5 times per day, providing good coverage of this important region for almost 15 months.

[7] The electron data used in this study were collected by the Medium Electrons A (MEA) experiment. This instrument, which used momentum analysis in a solenoidal field, had 17 energy channels ranging from 153 keV to 1.58 MeV [*Vampola et al.*, 1992]. The wave data used in this study were provided by the Plasma Wave Experiment. This experiment provided measurements of electric fields from 5.6 Hz to 400 kHz, using a 100 m tip-to-tip long wire antenna, with a dynamic range covering a factor of at least 10^5 in amplitude [*Anderson et al.*, 1992]. The electric field detector was thus able to detect waves from below the lower hybrid resonance frequency (f_{LHR}) to well above the upper hybrid resonance frequency (f_{UHR}) for a large fraction of each orbit.

3. Data Analysis

3.1. CRRES Database

[8] In order to study electron loss rates and the role of plasmaspheric hiss in the loss process, we constructed a database from the wave and particle data. The electron differential number flux perpendicular to the ambient magnetic field for each energy level of the MEA instrument and the ratio f_{pe}/f_{ce}, together with the magnetic field intensities in the range $0.1 \leq f \leq 2$ kHz and the electric field intensities in the range $f_{ce} < f < 2f_{ce}$ were rebinned as a function of half orbit (outbound and inbound) and L in steps of 0.1 L as detailed by *Meredith et al.* [2004]. The data were recorded together with the universal time (UT), magnetic latitude (λ_m), magnetic local time (MLT), and time spent in each bin with the same resolution. The subsequent analysis of the particle data was restricted to the equatorial perpendicular fluxes, defined to be observations within ±15° of the magnetic equator to reduce latitudinal effects in measurements of the perpendicular flux and the ratio f_{pe}/f_{ce}. If we assume a dipole field then this criterion restricts the analysis to equatorial pitch angles, α_{eq}, in the range ($60° \leq \alpha_{eq} \leq 120°$).

3.2. Determination of the Loss Timescale

[9] During quiet periods the energetic electron flux, J, often exhibits an exponential decay. To quantify the decay and compare results for different energies and L shells, we have calculated a loss timescale, τ, by fitting an exponential function of the form $J = Ae^{-(t/\tau)}$ to periods of gradual decay. To prevent the fits from being dominated by the most intense fluxes, we obtain the decay time constant by fitting a linear function to the natural logarithm of the flux. The fitting intervals are selected automatically to prevent ob-

server bias from influencing the results. We measure the strength of the linear relationship between the natural logarithm of the flux and the decay time using the Pearson correlation coefficient. The value of this coefficient varies from −1 to +1 with −1 indicating a perfect negative (inverse) correlation, 0 no correlation, and +1 a perfect positive correlation. We proceed as follows. The Pearson correlation coefficient is determined for the first ten points. If the Pearson coefficient is negative with an absolute value less than 0.95 or positive the fit is discarded and the starting point is incremented by one point. The process is then repeated throughout the data set. When the Pearson correlation coefficient is negative with an absolute value greater than 0.95 the number of points included in the fit is increased in unit increments up to a maximum of 75 points. The fitting interval is then chosen to be the fit with the largest absolute value of the Pearson coefficient. The whole process is then repeated starting from the next point after the fitting interval. The process is repeated for the whole data set as a function of time for selected energies and L shells.

[10] We tested the sensitivity of the technique to the minimum number of points in the fit by using a minimum of five points as compared with ten and found that the results were relatively insensitive to the minimum number of point in the fit. The nature of the fitting technique is such that we do not fit to intervals with less than five points which corresponds to a minimum duration of approximately 25 hours due to the orbital period of CRRES. Periods of fast decay, associated with the main phase of geomagnetic storms, are thus excluded from the fits and we concentrate on the periods of more gradual decay following enhanced magnetic activity.

3.3. Determination of the Plasma Environment

[11] The ratio of the electron plasma frequency, f_{pe}, to the electron gyrofrequency, f_{ce}, is an important parameter for electron acceleration and loss in the inner magnetosphere [*Summers et al.*, 1998; *Horne*, 2002]. Given the presence of the appropriate whistler mode waves, low values of this ratio are associated with the plasma trough and energy and pitch-angle diffusion [*Summers et al.*, 1998; *Horne et al.*, 2003]. High values of this ratio are associated with the plasmasphere, pitch-angle scattering and subsequent loss to the atmosphere [*Lyons et al.*, 1972; *Summers et al.*, 1998; *Summers*, 2005].

[12] Loss processes inside the plasmapause may be very different to those outside and have different relative importance. It is therefore helpful to identify the location of the observations with respect to the plasmapause, which can be inferred from measurements of the ratio of f_{pe}/f_{ce}. In order to construct their empirical plasmaspheric density model, *Sheeley et al.* [2001] adopted an L-shell dependent boundary number density, given by $n_b = 10^7(6.6/L)^4$ m^{-3}, to separate plasmaspheric-like and trough-like values. Densities below n_b were considered trough-like and densities above n_b were considered to be plasmaspheric-like. We use the same criterion and express the boundary ratio $(f_{pe}/f_{ce})_b$ in terms of the boundary number density, n_b, and the local magnetic field strength, B, as

$$\left(f_{pe}/f_{ce}\right)_b = \sqrt{(n_b m_e/\epsilon_0 B^2)} \quad (1)$$

If we assume a dipole field, then

$$B = B_{eq}\sqrt{(1+3\cos^2\theta)}/L^3\sin^6\theta \quad (2)$$

where B_{eq} is the mean value of the magnetic field on the equator at the surface of the Earth, and θ is the colatitude. Substituting in values for the appropriate constants, and keeping the plasma density constant with magnetic latitude, we obtain

$$\left(f_{pe}/f_{ce}\right)_b = 1.416L\sin^6\theta/\sqrt{(1+3\cos^2\theta)} \quad (3)$$

The boundary value, separating the plasmasphere-like values from trough-like values, for measurements made within 15° of the magnetic equator on a given geomagnetic field line thus lies in the range $1.23L \pm 0.18L$. Typically, in the plasmasphere, the ratio f_{pe}/f_{ce} is much larger than the boundary value, and, in the plasma trough, the ratio f_{pe}/f_{ce} is much smaller than the boundary value.

4. Results

4.1. $L = 3.55$

[13] The Kp index and the equatorial perpendicular differential number flux of 1.09 MeV electrons at $L = 3.55$ are plotted as a function of day number from 01/01/90 for the entire CRRES mission in Figure 1. The Kp index has been smoothed using a 15 hour running mean and the electron data have been color-coded according to the value of the ratio f_{pe}/f_{ce}. In the equatorial region at $L = 3.55$, $(f_{pe}/f_{ce})_b = 4.4 \pm 0.6$ so that measurements made when f_{pe}/f_{ce} is above or below ∼4.4 may be regarded as plasmaphere-like or trough-like, respectively.

[14] Large increases in the flux of relativistic electrons are associated with increased magnetic activity as monitored by the Kp index, and, in particular, when $Kp > 5$. These events are associated with magnetic storms, as monitored by the Dst index. The increase can be very rapid, such as the event on day number 332, or may take place over a timescale of days. The very rapid events may be attributed to either shock acceleration [*Li et al.*, 1993; *Hudson et al.*, 1997] or the inward movement of the inner edge of the outer belt. The longer-lasting flux increases take place over a period of 2–4 days and are associated with low values of f_{pe}/f_{ce} and hence the trough region. These events are known to be associated with enhanced levels of magnetic activity, enhanced chorus activity, and enhanced fluxes of seed electrons [e.g., *Meredith et al.*, 2002a, 2002b, 2003b; *Miyoshi et al.*, 2003].

[15] In the absence of further significant magnetic activity ($Kp < \sim 3$) the elevated poststorm relativistic electron fluxes gradually decay to quiet time values. During quiet periods the fluxes may fall by as much as two orders of magnitude over a period of ∼20 days. The best fits to the selected decay periods are overplotted on the data and yield a decay time constant of 5.7 ± 0.6 days, where the quoted error, here and henceforth, is the error of the mean. These periods of gradual decay are all associated with elevated values of the ratio f_{pe}/f_{ce}. The average value of f_{pe}/f_{ce} for the fitting intervals is 9.5 ± 0.2, indicating that these periods of gradual flux decay take place largely in the plasmasphere. The

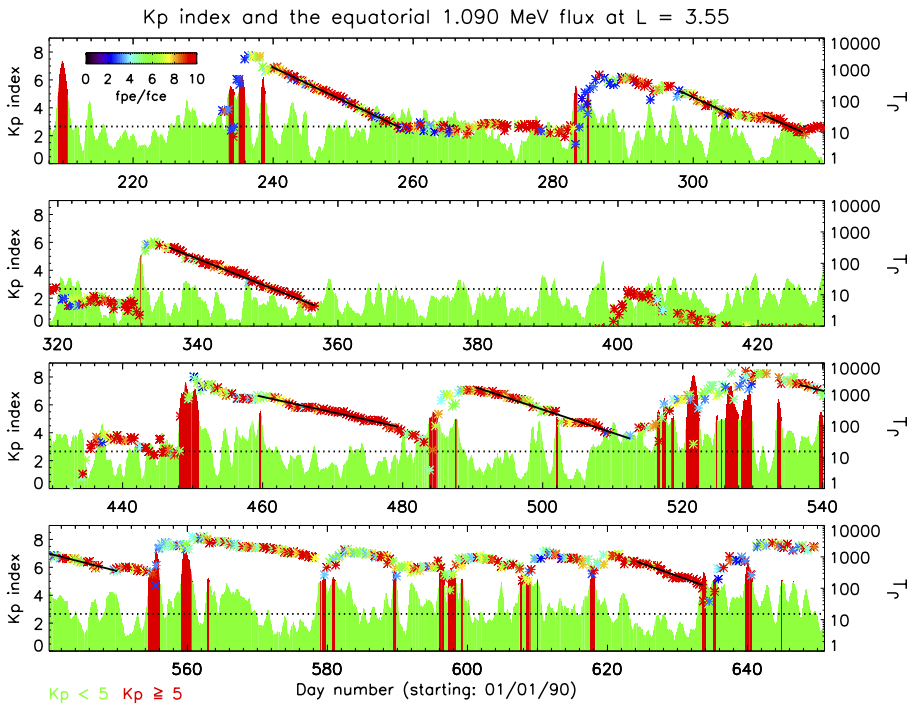

Figure 1. The *Kp* index and the equatorial perpendicular differential number flux of 1.09 MeV electrons at $L = 3.55$ as a function of day number for the entire CRRES mission. The *Kp* index has been smoothed using a 15-hour running mean and the data points are color-coded according to the value of f_{pe}/f_{ce} at the time of the measurement. The *Kp* value of 3^- is represented by the horizontal dashed line. The best fits to the selected decay periods are overplotted on the data.

average value of the *Kp* index during the intervals of decay is 2.23 ± 0.02, indicative of relatively quiet magnetic activity.

4.2. $L = 4.55$

[16] The *Kp* index and the equatorial perpendicular differential number flux of 1.09 MeV electrons at $L = 4.55$ are plotted as a function of day number from 01/01/90 in Figure 2. In the equatorial region at $L = 4.55$ measurements made when f_{pe}/f_{ce} is above or below ~5.6 may be regarded as plasmaphere-like or trough-like, respectively. At $L = 4.55$ we see a larger number of flux enhancements due to the fact that weaker storms can result in flux increases at larger L. The increases are again associated with low values of f_{pe}/f_{ce}, typically $f_{pe}/f_{ce} < 4$. At $L = 4.55$ the decay time-constant is 5.3 ± 0.6 days, comparable to the timescale at $L = 3.55$. The average value of f_{pe}/f_{ce} during the decay periods is 11.0 ± 0.4, consistent with electron decay in this region taking place in the plasmasphere. The average value of the *Kp* index during the intervals of decay is 1.83 ± 0.02, indicative of relatively quiet magnetic activity.

[17] The *Kp* index and the equatorial perpendicular electron differential number flux of 214 keV electrons at $L = 4.55$ are shown for comparison with the MeV electrons in Figure 3. During high magnetic activity the ratio f_{pe}/f_{ce} is low denoting the plasma trough. The flux levels also tend remain high. The loss timescales are more rapid than at 1.09 MeV, and, during quiet periods, the fluxes may fall by as much as two orders of magnitude over a period of ~6 days. The best fits to the selected decay periods yield a decay time constant of 2.0 ± 0.1 days, a factor of 2.65 times faster than at 1.09 MeV. The average value of the ratio f_{pe}/f_{ce} for the fitting intervals is 9.9 ± 0.3, consistent with electron decay at this energy also occurring in the plasmasphere. The intervals of decay again occur during quiet magnetic conditions when the average value of the *Kp* index is 1.7 ± 0.1.

4.3. $3 \leq L \leq 5$

[18] The analysis was repeated for different energies and L shells and the resulting decay timescales are plotted as a function of energy and L shell for the region $3 \leq L \leq 5$ in Figure 4. At 1.09 MeV the decay timescales lie in the range 5.5–6.5 days and show little variation with L shell. In contrast, at 510 keV the decay timescales are less, ranging from 2.5 to 5.5 days, and display a general tendency to increase with increasing L for $L > 3.6$. The shortest timescales are seen at 214 keV, ranging from 1.5 to 3.5 days, and display a tendency to increase with increasing L for $L > 4$. Beyond $L = \sim 5$ the data exhibit more variability and it is not possible to calculate reliable average loss timescales using our fitting criteria. The fitting technique also breaks down inside $L = 3.3$ for 214 keV electrons, due to increased scatter between neighboring data points.

[19] The average value of the ratio f_{pe}/f_{ce} during the selected intervals of gradual decay for 214 keV, 510 keV, and 1.09 MeV electrons at each L shell studied is shown in Figure 5. The dashed line represents the boundary value between the trough and plasmaspheric-like material with trough-like material below the line and plasmaspheric-like material above the line. Here f_{pe}/f_{ce} lies well above the line for all energies and L shells suggesting that the intervals of gradual decay take place in the plasmasphere.

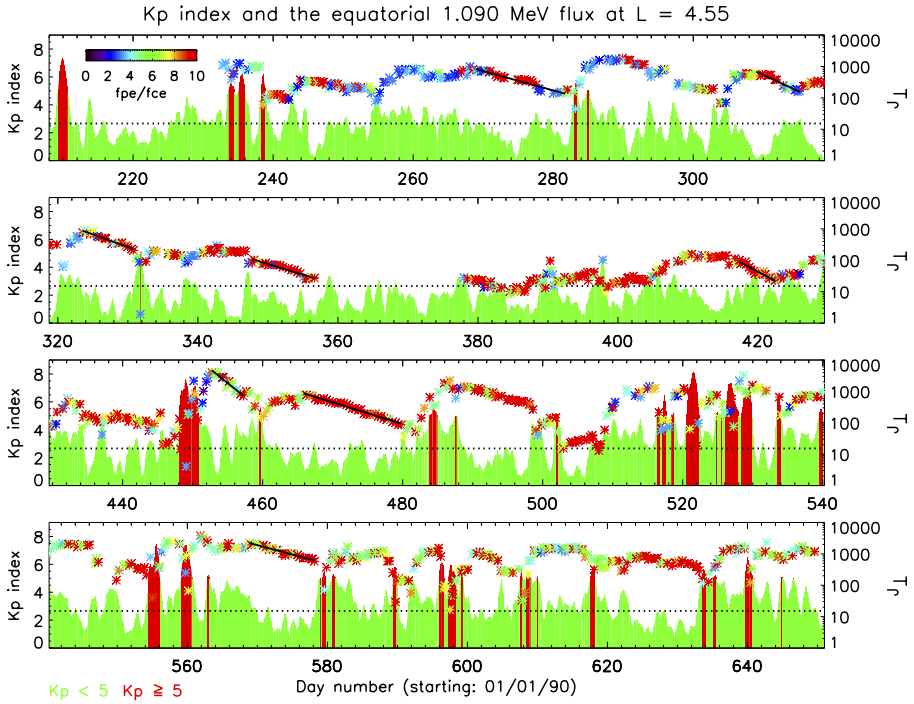

Figure 2. The *Kp* index and the equatorial perpendicular differential number flux of 1.09 MeV electrons at $L = 4.55$ in the same format as Figure 1.

[20] The average value of the *Kp* index during the selected intervals of gradual decay for 214 keV, 510 keV, and 1.09 MeV electrons at each *L* shell studied is shown in Figure 6. The intervals of decay are associated with low values of *Kp* ($Kp \leq 3^-$), indicative of quiet time conditions. There is also a tendency for the average value of *Kp* during the decay periods to decrease with increasing *L* shell. Since the quiet-time decay takes place largely in the plasmasphere, quiet-time decay only becomes possible at a given location once the plasmapause has expanded beyond the location, which can only occur when *Kp* becomes small [*Carpenter and Anderson*, 1992]. On average, quieter

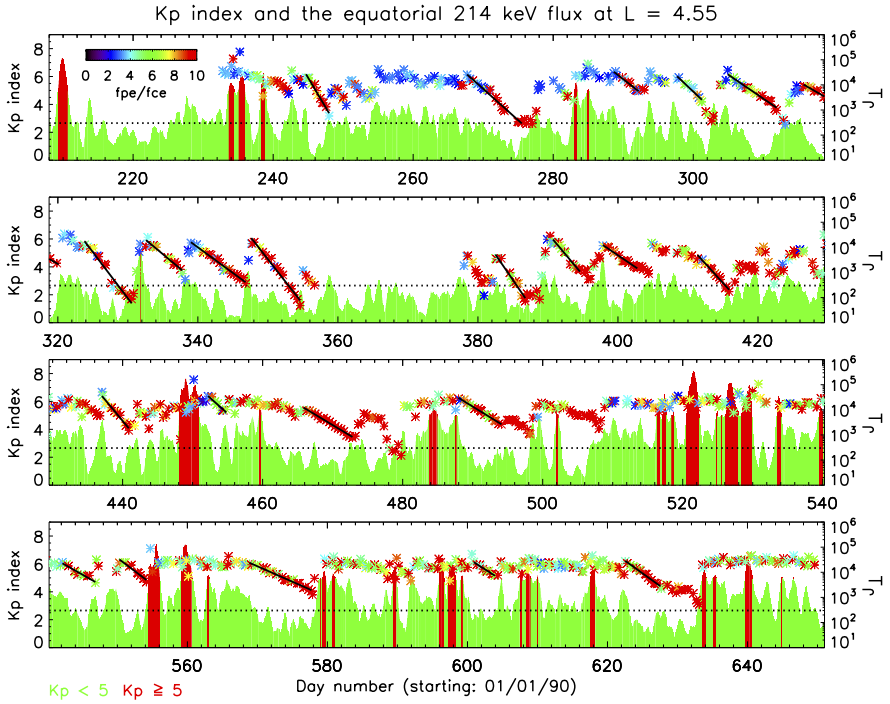

Figure 3. The *Kp* index and the equatorial perpendicular differential number flux of 214 keV electrons at $L = 4.55$ in the same format as Figure 1.

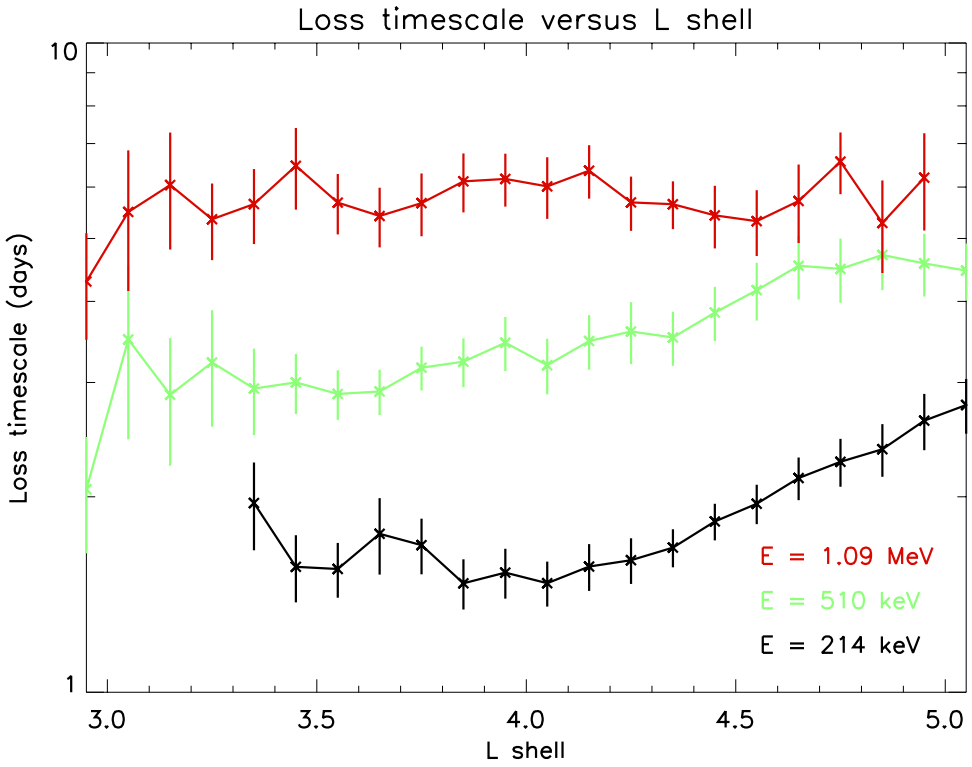

Figure 4. Measured electron loss timescales versus L shell for 214 keV, 510 keV, and 1.09 MeV electrons.

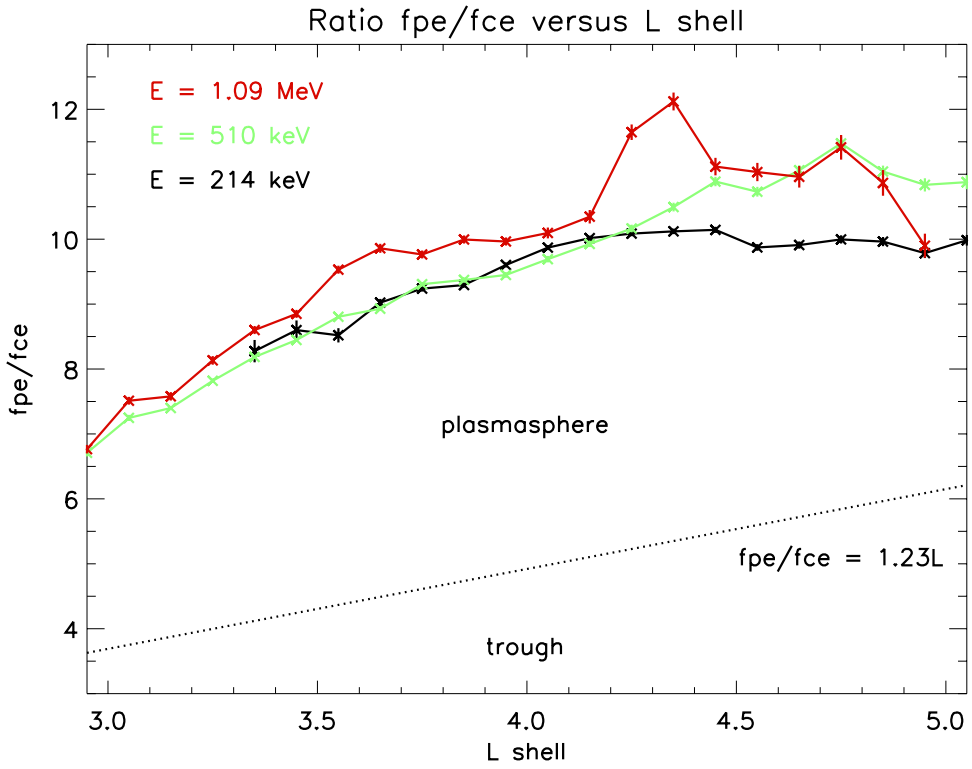

Figure 5. The average value of f_{pe}/f_{ce} during the selected intervals of decay versus L shell for 214 keV, 510 keV, and 1.09 MeV electrons. The dashed line represents the boundary value between trough and plasmaspheric-like material.

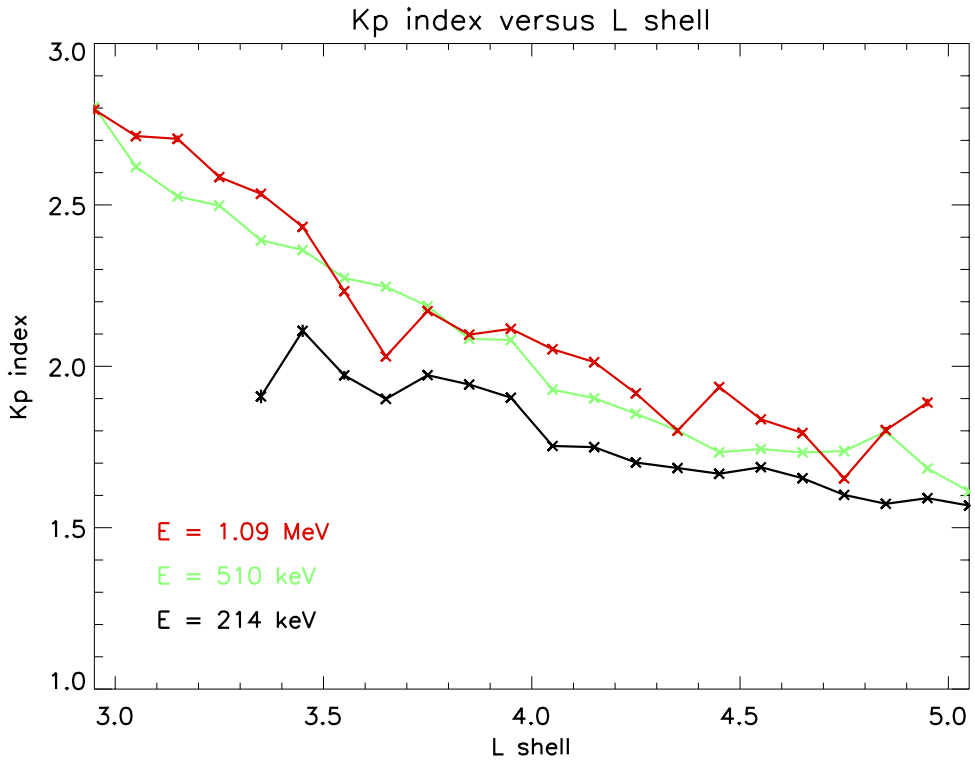

Figure 6. The average value of the *Kp* index during the selected intervals of decay versus *L* shell for 214 keV, 510 keV, and 1.09 MeV electrons.

magnetic conditions and smaller values of *Kp* are required with increasing *L* which explains the observed trend.

5. Loss Mechanisms

[21] The observations of gradual periods of electron loss lasting for several days or more are largely associated with high values of f_{pe}/f_{ce} and hence take place in the plasmasphere. While observations on the duskside cannot confirm that the electrons spend all of their drift orbits inside the plasmapause, the observations of loss associated with large values of f_{pe}/f_{ce} on the dawnside suggest that during the periods of gradual decay, the electrons do indeed remain inside the plasmapause for the majority of their drift orbits.

[22] The chorus waves, thought to play a role in the acceleration of electrons to relativistic energies in the outer radiation belt, tend to be confined to the low-density regions outside of the plasmapause and so are unlikely to play a role in electron loss in the plasmasphere. On the other hand, electromagnetic ion cyclotron (EMIC) waves, plasmaspheric hiss, lightning-generated whistlers, and VLF transmitter signals are observed in the plasmasphere and may all contribute to pitch-angle scattering and subsequent electron loss in this region [e.g., *Albert*, 2003; *Summers and Thorne*, 2003; *Thorne et al.*, 2005b; *Summers*, 2005].

[23] Electromagnetic ion cyclotron waves, which propagate in bands below the proton gyrofrequency, are able to interact with energetic electrons resulting in pitch-angle scattering and loss to the atmosphere [e.g., *Summers and Thorne*, 2003; *Albert*, 2003]. However, electron minimum resonant energies are only observed to fall below 2 MeV in the region $L > 4.5$ when $f_{pe}/f_{ce} > 10$ and largely occur on the duskside [*Meredith et al.*, 2003c]. Furthermore, these lower-energy scattering events tend to be associated with magnetic storms. It is therefore unlikely that EMIC waves will play the most significant role in the loss of electrons with energies in the range 100 keV $< E <$ 1 MeV during the relatively quiet periods associated with gradual electron decay and, in particular, inside of $L = 4.5$.

[24] Plasmaspheric hiss is a broadband, structureless emission which occurs in the frequency range from 100 Hz to several kHz. This whistler mode emission is observed inside of the plasmapause and is most intense during storms, although the emissions also persist during relatively quiet times [e.g., *Smith et al.*, 1974; *Thorne et al.*, 1977; *Meredith et al.*, 2004]. The minimum resonant energies for a band of hiss in the range $3.0 \leq L \leq 5.0$ are typically less than 100 keV, and thus the waves can resonate with electrons with $E \geq 100$ keV. Plasmaspheric hiss could thus play an important role in electron loss inside the plasmapause and, in particular, to the gradual loss observed when quiet periods follow geomagnetic storms.

6. Estimation of Loss Rates Due to Plasmaspheric Hiss

[25] We investigate the role of plasmaspheric hiss as a loss process using wave observations from the CRRES spacecraft to calculate pitch-angle diffusion rates for electrons. The diffusion rates are calculated using the PADIE (Pitch Angle and Energy Diffusion of Ions and Electrons) code [*Glauert and Horne*, 2005].

[26] Since resonant scattering by hiss is not sensitive to the ion composition, an electron/proton plasma is assumed.

The determination of the diffusion coefficients then requires knowledge of the distribution of the wave power spectral density with frequency and wave normal angle, together with the ratio f_{pe}/f_{ce}, wave mode, and the number of resonances. We calculate the bounce-averaged pitch-angle diffusion coefficients for whistler mode hiss for Landau (n = 0) and ±5 cyclotron harmonic resonances.

[27] The waves are assumed to have a Gaussian frequency distribution given by

$$B^2(\omega) = \begin{cases} A^2 \exp\left(-\left(\frac{\omega-\omega_m}{\delta\omega}\right)^2\right) & \omega_{lc} \le \omega \le \omega_{uc} \\ 0 & \text{otherwise,} \end{cases} \quad (4)$$

where B^2 is the power spectral density of wave magnetic field (in T^2 Hz^{-1}), ω_m and $\delta\omega$ are the frequency of maximum wave power and bandwidth, respectively, ω_{lc} and ω_{uc} are lower and upper bounds to the wave spectrum outside which the wave power is zero, and A^2 is a normalization constant given by

$$A^2 = \frac{|B_w|^2}{\delta\omega}\frac{2}{\sqrt{\pi}}\left[\text{erf}\left(\frac{\omega_m-\omega_{lc}}{\delta\omega}\right)+\text{erf}\left(\frac{\omega_{uc}-\omega_m}{\delta\omega}\right)\right]^{-1} \quad (5)$$

where B_w is the wave amplitude in units of Tesla. The distribution of wave normal angles ψ is also assumed to be Gaussian, given by

$$g(X) = \begin{cases} \exp\left(-\left(\frac{X-X_m}{\delta X}\right)^2\right) & X_{lc} \le X \le X_{uc} \\ 0 & \text{otherwise,} \end{cases} \quad (6)$$

where $X = \tan(\psi)$, δX is the angular width, X_m is the peak, and X_{lc} and X_{uc} are the lower and upper bounds to the wave normal distribution outside of which the wave power is zero.

[28] Once the pitch-angle diffusion rate is calculated, the timescale for the electrons to pitch-angle scatter into the loss cone can be determined. Following previous work [*Lyons et al.*, 1972; *Albert*, 1994], we assume that the electron distribution function, f, satisfies the one-dimensional pitch-angle diffusion equation,

$$\frac{\partial f}{\partial t} = \frac{1}{T\sin 2\alpha_0}\left(\frac{\partial}{\partial\alpha_0}\left(\langle D_{\alpha\alpha}\rangle T\sin 2\alpha_0\frac{\partial f}{\partial\alpha_0}\right)\right) \quad (7)$$

where α_0 is the equatorial pitch-angle, $\langle D_{\alpha\alpha}(\alpha_0)\rangle$ is the bounce-averaged pitch-angle diffusion coefficient in units of s^{-1}, and

$$T(\alpha_0) = 1.30 - 0.56\sin\alpha_0 \quad (8)$$

is an approximation to the mirror latitude dependence of the bounce period.

[29] By assuming that f can be factorized into time-dependent and pitch-angle dependent functions,

$$f(\alpha_0, t) = F(t)g(\alpha_0), \quad (9)$$

and that the precipitation lifetime, τ is given by

$$\tau = \frac{-F}{dF/dt}, \quad (10)$$

equation (7) becomes

$$\frac{\partial}{\partial\alpha_0}\left(\langle D_{\alpha\alpha}\rangle T\sin 2\alpha_0\frac{dg}{d\alpha_0}\right)+\frac{T\sin 2\alpha_0}{\tau}g = 0. \quad (11)$$

Equation (11), together with the boundary conditions

$$g(\alpha_L) = 0, \quad (12)$$

$$\frac{dg}{d\alpha_0}\left(\frac{\pi}{2}\right) = 0, \quad (13)$$

$$2\int_{\alpha_L}^{\frac{\pi}{2}} g\sin\alpha_0 d\alpha_0 = 1, \quad (14)$$

where α_L is the loss cone pitch-angle, can be cast as a two-point boundary value problem in four variables [*Albert*, 1994], which can be solved to obtain the lifetime, τ. We solved this boundary value problem with a routine from the NAG library, D02GAF, which uses a finite difference method combined with a deferred correction technique and a Newton iteration.

6.1. Wave Model

[30] We use a model based on CRRES observations for the plasmaspheric hiss wave intensities. Since whistler mode chorus waves can fall into the hiss band outside of $L \sim 3.5$, we adopt a criterion based on the wave amplitude in the ECH band ($f_{ce} < f < 2f_{ce}$) to distinguish between plasmaspheric hiss and chorus. Specifically, we use the criterion that the ECH wave amplitude for frequencies in the range $f_{ce} < f < 2f_{ce}$ must be less than 0.0005 mV m^{-1} in order for wave emissions below f_{ce} in the frequency range $0.1 \le f \le 2$ kHz to be identified as plasmaspheric hiss [*Meredith et al.*, 2004].

[31] Energetic electrons ($E > 200$ keV) in the Earth's outer radiation belt drift around the Earth on timescales of the order of 1 hour or less which means that they typically complete many orbits during the periods of gradual decay. The electrons interact with plasmaspheric hiss while their drift orbit lies inside the plasmapause which, during quiet conditions in the region $3 < L < 5$, is typically the entire orbit. Therefore we require a global model of the hiss intensities to obtain an estimate of the loss rates. Hiss intensities vary as a function of spatial location and magnetic activity [*Meredith et al.*, 2004]. Since the intervals of gradual decay take place during quiet periods ($Kp < 3^-$), the survey is restricted to measurements taken when the instantaneous value of Kp is less than 3^-. The average value of the intensity of plasmaspheric hiss during such conditions is plotted as a function of L shell and magnetic local time in Figure 7. The hiss intensities peak on the dayside with intensities typically of the order of 1000 pT^2 over a range of L shells from $L = 2$ to $L = 4$ from 0600 to 2100 MLT. Lower intensities are seen near midnight and at larger L shells. The latitudinal variation of the plasmaspheric hiss intensities averaged over all MLT are shown in the top panels of Figure 8. The hiss intensities tend to peak near the equator ($\lambda_m < 5°$) and at higher latitudes ($\lambda_m > 15°$).

[32] To reduce the complexity of the calculations, we create a basic model of the plasmaspheric hiss intensities as

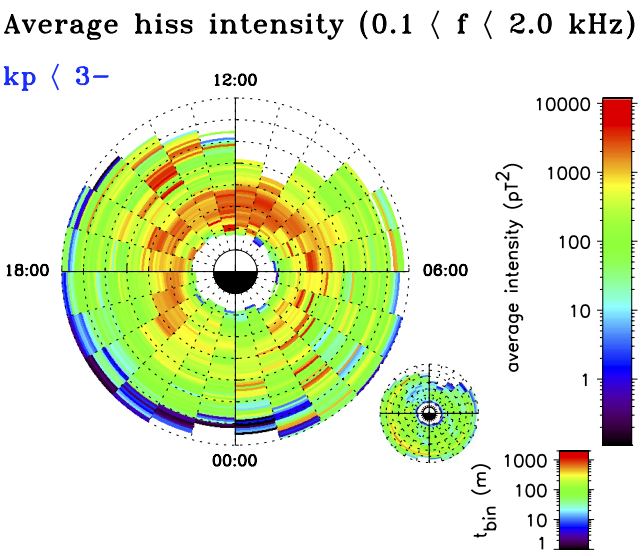

Figure 7. The average hiss magnetic field wave intensity as a function of L and MLT for quiet conditions ($Kp < 3^-$). The sampling distribution, color-coded to show the number of minutes in each bin, $t_b(m)$, is shown in the small panel.

a function of L shell by averaging the intensities during quiet conditions in steps of $0.2L$ first over magnetic latitude and then over magnetic local time. The model wave magnetic field intensities are plotted as a function of L shell in Figure 9a and included in the second column of Table 1. The model intensities have a peak value of 1359 pT^2 at $L = 3.3$ falling to 1190 pT^2 at $L = 3.0$ and 380 pT^2 at $L = 5.0$.

[33] The mean value of the ratio of f_{pe}/f_{ce} is plotted as a function of magnetic latitude for the same conditions and regions in the bottom panels of Figure 8. Along any given L shell the ratio f_{pe}/f_{ce} tends to decrease with increasing latitude due to the increasing field strength with magnetic latitude. At a given magnetic latitude, the ratio f_{pe}/f_{ce} tends to increase with increasing L shell. The dashed lines show the model values, determined from least squares best fits to the data, assuming a dipole field and constant density. The equatorial values of the best fit to f_{pe}/f_{ce} are plotted as a function of L shell in Figure 9b and are tabulated in the fifth column of Table 1. The equatorial values of the ratio f_{pe}/f_{ce} increase from 8.9 at $L = 3.0$ to 13.0 at $L = 5.0$.

[34] Plasmaspheric hiss appears to propagate over a broad range of wave normal angles with predominantly field-aligned propagation near the geomagnetic equator and more oblique propagation at higher latitudes [*Parrot and Lefeuvre*, 1986; *Hayakawa et al.*, 1986; *Santolik et al.*, 2001]. For example, in the equatorial region ($\lambda_m < 10°$), *Parrot and Lefeuvre* [1986] found two populations of wave normal angles, one lying in the range $0° \leq \psi \leq 30°$, the other in the range $40° \leq \psi \leq 60°$. At higher latitudes ($\lambda_m > 20°$), most of the waves had larger wave normal angles in the range $55° \leq \psi \leq 85°$. To investigate the effect of the wave normal angle on the precipitation lifetimes, we use three different angular distributions of hiss, chosen to be representative of these observations (Table 2).

[35] The conversion from electric field intensity to magnetic field intensity assumes parallel propagation [*Meredith et al.*, 2004]. We calculate approximate intensities for propagation at 52° and 80° using the cold plasma dispersion solver in the HOTRAY code [*Horne*, 1989] assuming a frequency of 0.55 kHz and using the modeled values of f_{pe}/f_{ce}. The derived intensities are tabulated in the third and fourth columns of Table 1 and are typically a factor of 1.6 lower for a wave normal angle of 52° and a factor of 5 lower for a wave normal angle of 80°.

[36] We calculate the bounce-averaged diffusion rate which takes into account the scattering of particles in pitch angle over the complete range of latitudes between the

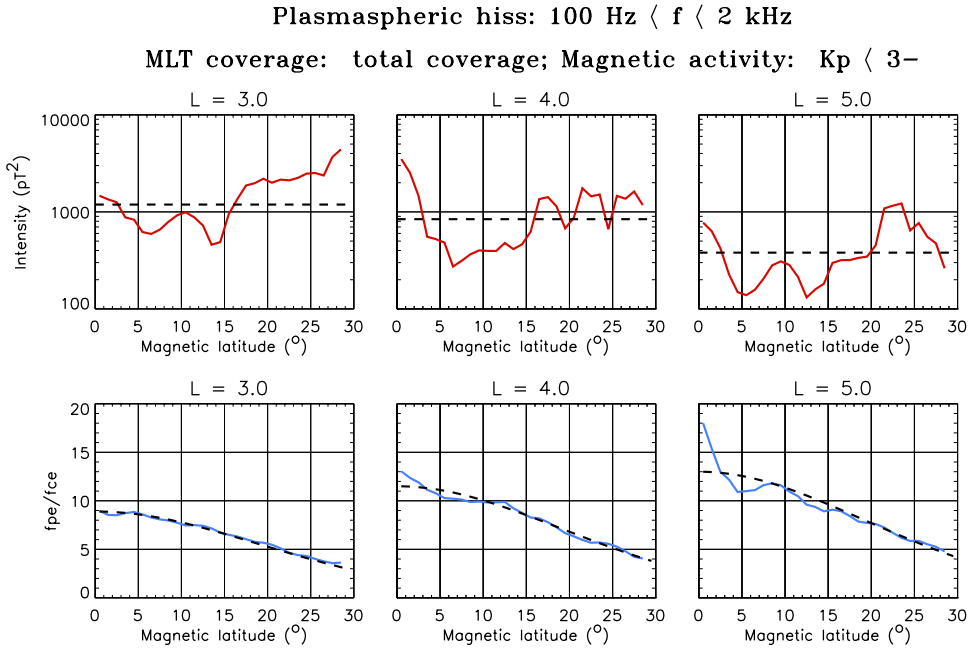

Figure 8. (top) The average hiss magnetic field wave intensity and (bottom) the ratio f_{pe}/f_{ce} for quiet times at different L shells. The model values are shown by the dashed lines.

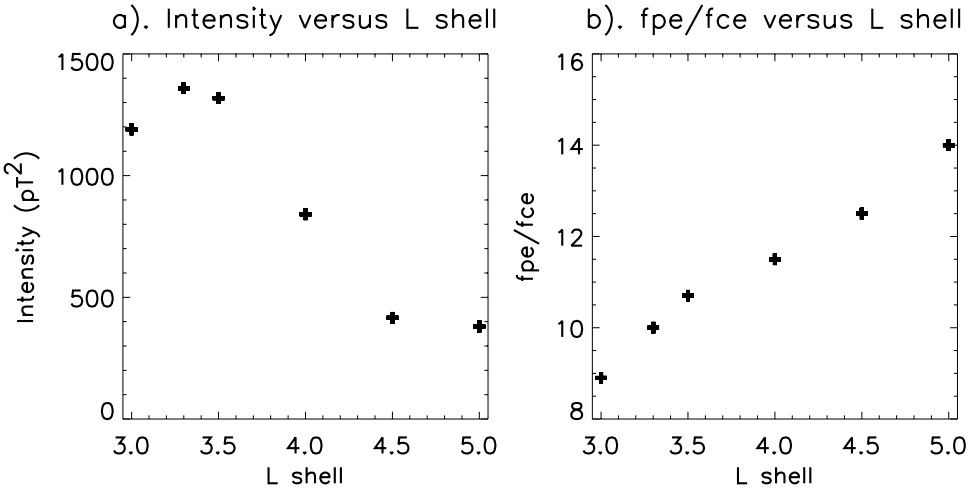

Figure 9. (a) The modeled value of the plasmaspheric hiss intensity as a function of L shell. (b) The modeled value of the ratio f_{pe}/f_{ce} at the magnetic equator as a function of L shell.

particle's mirror points. In general the waves resonate with higher-energy electrons at higher latitudes and will tend to scatter higher-energy electrons into the loss cone at higher latitudes. This is shown in more detail in Figure 2 of *Horne and Thorne* [2003] for the case of chorus waves. We assume a Gaussian frequency distribution centered on 0.55 kHz with a bandwidth of 0.3 kHz and lower and upper cutoff's of 0.1 kHz and 2.0 kHz, respectively.

6.2. Results

[37] Figure 10 shows the loss timescale as a function of L shell for 214 keV electrons (lower panel), 510 keV electrons (middle panel), and 1.09 MeV electrons (upper panel). The vertical bars denote the range covered by plus or minus one standard deviation of the mean value of the measured loss timescales. The pluses denote the model values. The results are shown for the three different angular distributions of hiss, blue for the small wave normal model, green for the medium wave normal model, and red for the large wave normal model.

[38] At 214 and 510 keV the small and medium wave normal models produce loss timescales that are consistent with the observed values in the regions $3.5 \leq L \leq 5.0$ and $3.0 \leq L \leq 5.0$, respectively. At 1.09 MeV both models fit the data well in the region $3.0 \leq L \leq 4.0$ but overestimate the loss timescales at larger L by a factor of $\sim$5. In comparison, the large wave normal model overestimates the loss timescales by an order of magnitude or more at all L shells and energies considered.

[39] The lowest loss timescales are obtained from the small wave normal model. The small and medium wave normal models produce loss timescales that tend to lie within a factor of two of each other, whereas the large wave normal model produces loss timescales that are typically an order of magnitude larger.

7. Discussion

[40] The energetic outer zone electron loss timescales during low geomagnetic activity derived from the CRRES MEA data compare favorably with those presented in previous studies. For example, loss timescales derived from the OV3-3 satellite in the region $3 < L < 4$ following a period of gradual decay following the intense storm of 4 September 1966 range from 2.6 to 5.1 days for 475 keV electrons and from 5.1 to 8.5 days for 957 keV electrons [*Lyons et al.*, 1972]. Furthermore, the loss timescales derived from the OGO-5 satellite in the region $3 < L < 5$ following the moderate storm of 11 June 1968 range from 1.3 to 2.8 days for 266 keV electrons, from 1.3 to 5.0 days for 475 keV electrons, and from 1.7 to 7.8 days for 866 keV electrons [*West et al.*, 1981]. More recently, *Baker et al.* [1994] conducted a superposed epoch analysis of 1 year of SAMPEX data and estimated loss timescales for electrons with energies greater than 400 keV in the region $2.5 < L < 5$ of between 5 and 10 days. While a direct comparison with a specific CRRES energy channel is not possible in this case the range of values has some overlap with the range of values determined from CRRES at 510 keV and considerable overlap at 1.09 MeV (Figure 10). *Albert* [2000] studied the 9 October 1990 storm using CRRES MEA count rate data and showed that the loss timescale of 510 keV electrons had a minimum of 1.6 days at $L = 3.2$, rising to 4.6 days at $L = 2.6$ and 2.6 days at $L = 3.7$. *Seki et al.* [2005] used CRRES and Akebono data to estimate the loss timescales at $L = 3.25$ following the strong magnetic storm of 26 August 1990. The loss timescales derived from the CRRES MEA data ranged from to 3.1 days for 976 keV electrons to 5.3 days for 1.58 MeV electrons and the loss timescale derived from the Akebono satellite was higher, at 8.3 days for electrons with energies in the range 950–2500 keV. The longer timescale observed by Akebono was attributed to the slower decay of high-energy electrons within the instrumental energy range. The lifetimes derived in previous studies are thus largely consistent with the range of lifetimes determined in our study (Figure 10), both as a function of energy and L shell.

Table 1. Model Parameters

L	$B^2_{w,0}(pT^2)$	$B^2_{w,52}(pT^2)$	$B^2_{w,80}(pT^2)$	f_{pe}/f_{ce}
3.0	1190	721	189	8.9
3.3	1359	829	228	10.0
3.5	1318	808	230	10.7
4.0	841	519	163	11.5
4.5	416	260	93	12.5
5.0	380	242	107	13.0

Table 2. Wave Normal Models

Model	ψ	X_m	δX	X_{lc}	X_{uc}
Small wave normal model	0.0	0.00	0.36	0.00	0.58
Medium wave normal model	52.0	1.28	0.27	0.84	1.73
Large wave normal model	80.0	5.67	2.74	1.43	11.4

[41] *Albert* [1999] calculated plasmaspheric lifetimes for the region $1.5 < L < 5.0$ using the parameter values of *Abel and Thorne* [1998] for whistler mode waves due to hiss, lightning, and VLF transmitters. The lifetimes at 200 keV had a minimum of ~14 days at $L = 3.5$, increasing to ~50 days at $L = 3$ and ~20 days at $L = 5$. At 1 MeV they had a minimum of ~50 days at $L = 3$ rising to >400 days at $L = 2$ and ~200 days at $L = 5$. The values of these modeled lifetimes are typically an order of magnitude larger than the experimental values derived in our study. For $L > 3$, *Abel and Thorne* [1998] used a hiss amplitude of 10 pT assumed to be present for 50% of the time corresponding to an average intensity of 25 pT^2. Our measured values of the hiss intensities have a peak value of 1359 pT^2 at $L = 3.3$, falling to 1190 pT^2 at $L = 3$ and 380 pT^2 at $L = 5$. The measured intensities presented here are thus over an order of magnitude larger than the hiss intensity used by *Abel and Thorne* [1998] and hence also by *Albert* [1999]. Since lifetimes scale inversely with wave intensities, the reason why the plasmaspheric lifetimes obtained by *Albert* [1999] are much larger than the experimental values is due to an underestimation of the hiss wave power.

[42] Our results suggest that plasmaspheric hiss propagating at small or intermediate wave normal angles is responsible for electron loss over a wide range of L shells and energies in high-density regions. The region where hiss dominates loss is energy-dependent, ranging from $3.5 \leq L \leq 5.0$ at 214 keV to $3.0 \leq L \leq 4.0$ at 1.09 MeV. The results show that plasmaspheric hiss with large wave normal angles does not contribute significantly to electron loss from the radiation belts in the regions shown.

[43] The lowest model lifetime for 214 keV electrons at $L = 3.3$ is a factor of ~3 higher than the experimental lifetime at $L = 3.35$. Unfortunately, the fitting technique used in this study breaks down at lower L for 214 keV electrons due to increased scatter between neighboring data points so that we cannot explore the discrepancy further in this paper. We note that other wave emissions, such as lightning-generated whistlers and VLF transmitters, become increasingly important at low L and will contribute to the loss timescales in this region [*Abel and Thorne*, 1998].

[44] Our calculated larger loss timescales at high energies at large L require further investigation. *Albert* [1994], using a highly simplified version of the dispersion relation and resonance condition following *Lyons et al.* [1972], found that the inclusion of higher-order cyclotron harmonics could decrease the loss timescales, for energies above 500 keV and L values greater than 3. In particular, he found that increasing the number of cyclotron harmonics from ±5 to ±100 decreased the 1 MeV loss timescale by a factor of ~2.3 at $L = 5$. We also considered the contribution from higher-order cyclotron harmonics, increasing the number of cyclotron harmonics to ±100. We did not find a significant contribution from these higher-order cyclotron harmonics for any of the models used in this study. Higher-order cyclotron resonant effects depend sensitively on the angular distribution of the waves and the ratio f_{pe}/f_{ce}. For example, at $L = 5$ our modeled equatorial value, based on observations, for the ratio f_{pe}/f_{ce} is 12.8 compared to the value of 26.9 used by *Albert* [1994]. For higher-order cyclotron harmonics ($|n| > 5$) to play a role the resonant frequencies associated with these harmonics must lie within the frequency band of the waves. In our models the wave frequencies associated with these higher-order harmonics all lie above the upper cutoff frequency for the range of energies and L shells studied. In contrast, in the study of *Albert* [1994] the wave frequencies associated with the higher-order harmonics fall in the frequency band of the waves for certain energy and L shell ranges and hence play a role in the diffusion process. Since we use observed values of the wave parameters and the ratio f_{pe}/f_{ce}, we conclude that higher harmonic effects are not significant.

[45] Loss by chorus waves, known as microburst precipitation, generally occurs outside the plasmapause in regions of lower density [*Thorne et al.*, 2005a, 2005b; *O'Brien et al.*, 2004]. Thus microburst precipitation could contribute to electron loss at large L if part of the electron drift orbit occurs outside the plasmapause. However, modeling studies

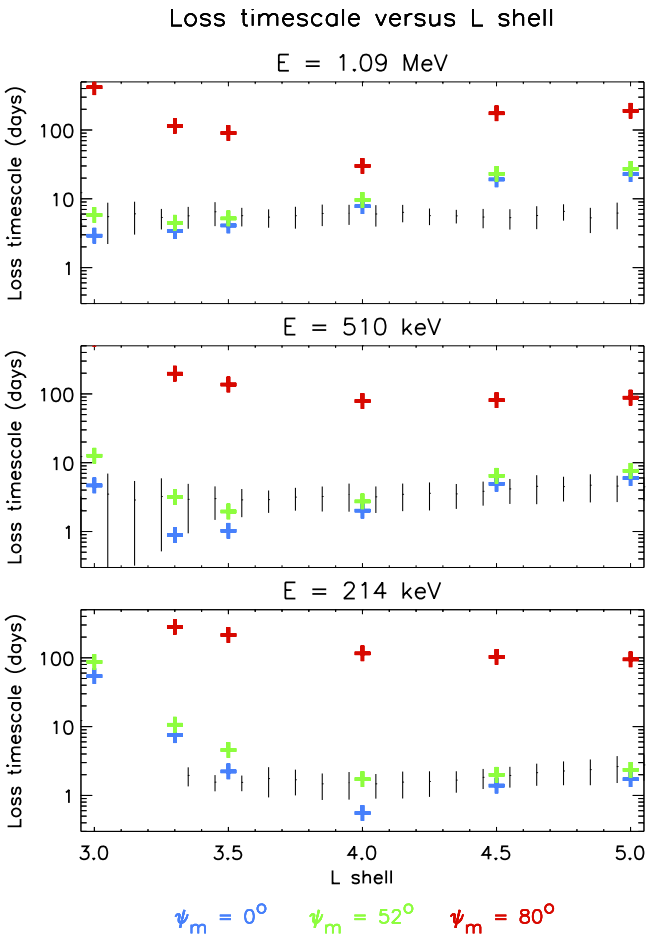

Figure 10. Electron loss timescales as a function of L shell for (top) $E = 1.09$ MeV, (middle) $E = 510$ keV, and (bottom) $E = 214$ keV. The measured values are denoted by the vertical lines and the model values by the pluses, color-coded to show the wave normal angle.

show that as chorus propagates along the magnetic field the resonant energies match $\sim$ MeV electrons at 20°–30° off the equator and are not well matched at the equator [*Horne and Thorne*, 2003]. At the equator the resonant energies are lower. Thus one may expect that if microburst precipitation were occurring, this would also reduce the loss timescales at lower energies. It appears that plasmaspheric hiss is adequate to explain the loss at lower energies. This does not rule out microburst loss provided the rate of loss at lower energies is dominated by hiss.

[46] EMIC waves can interact with MeV electrons [e.g., *Summers and Thorne*, 2003; *Albert*, 2003; *Summers*, 2005], particularly in regions of high density at larger L ($L > 4.5$) [*Meredith et al.*, 2003c], precisely the region where the MeV losses cannot be explained by resonant interactions with plasmaspheric hiss alone. Furthermore, *Albert* [2003] found that the addition of EMIC waves can greatly reduce the electron lifetimes determined by hiss alone. In addition, precipitation signatures from EMIC waves have been seen in plumes during substorm ion injections. These results suggest that EMIC waves in high-density regions, such as the duskside plasmapause and within drainage plumes, may contribute to the scattering of energetic electrons at larger L, and could, potentially, explain the loss rates in this region.

8. Conclusions

[47] We have analyzed CRRES particle data to determine the energetic electron decay timescales as a function of energy (214 keV $\leq E \leq$ 1.09 MeV) and L shell ($3 \leq L \leq 5$). The resulting timescales are compared with estimates of the decay timescales of plasmaspheric hiss using the PADIE code using CRRES wave data as input. Our principal results are as follows:

[48] 1. Gradual loss of energetic electrons in the region $3 \leq L \leq 5$ is observed to occur in quiet periods ($Kp < 3^-$) following enhanced magnetic activity.

[49] 2. Decay timescales range from 1.5–3.5 days for 214 keV electrons to 5.5–6.5 days for 1.09 MeV electrons.

[50] 3. The intervals of decay are associated with large average values of the ratio f_{pe}/f_{ce} (>7) and indicate that the decay takes place in the plasmasphere.

[51] 4. Modeling shows that plasmaspheric hiss propagating at small or intermediate wave normal angles can account for the electron loss rates over a wide range of energies and L shells. These regions are energy-dependent and range from $3.5 \leq L \leq 5.0$ at 214 keV to $3.0 \leq L \leq 4.0$ at 1.09 MeV.

[52] 5. Modeling shows that plasmaspheric hiss with very large wave normal angles does not contribute significantly to radiation belt electron loss.

[53] 6. At high energies, $E = 1.09$ MeV, plasmaspheric hiss propagating at small or intermediate wave normal angles overestimates the loss timescales by a factor of $\sim$5 at large L ($4.5 \leq L \leq 5.0$). Resonant wave-particle interactions with EMIC waves become important at MeV energies at larger L and high densities. We suggest that losses due to EMIC waves may play a significant role at larger L.

[54] **Acknowledgments.** We thank Al Vampola and Daniel Heynderickx for providing the MEA data used in this study and for many useful discussions. We also thank the NSSDC Omniweb for providing the Kp indices used in this paper. This work was supported in part by NSF grant ATM0402615 and NASA grant NNG04GN44G. D.S. acknowledges support from the Natural Sciences and Engineering Research Council of Canada under grant A-0621.

[55] Shadia Rifai Habbal thanks Takahiro Obara for his assistance in evaluating this paper.

References

Abel, B., and R. M. Thorne (1998), Electron scattering loss in the Earth's inner magnetosphere: 1. Dominant physical processes, *J. Geophys. Res.*, *103*, 2385.

Albert, J. M. (1994), Quasi-linear pitch-angle diffusion coefficients: Retaining higher harmonics, *J. Geophys. Res.*, *99*, 23,741.

Albert, J. M. (1999), Analysis of quasi-linear diffusion coefficients, *J. Geophys. Res.*, *104*, 2429.

Albert, J. M. (2000), Pitch-angle diffusion as seen by CRRES, *Adv. Space Res.*, *25*, 2343.

Albert, J. M. (2003), Evaluation of quasi-linear diffusion coefficients for EMIC waves in a multispecies plasma, *J. Geophys. Res.*, *108*(A6), 1249, doi:10.1029/2002JA009792.

Anderson, R. R., D. A. Gurnett, and D. L. Odem (1992), CRRES plasma wave experiment, *J. Spacecr. Rockets*, *29*, 570.

Baker, D. (2001), Satellite anomalies due to space storms, in *Space Storms and Space Weather Hazards*, edited by I. A. Daglis, pp. 251–284, chap. 10, Springer, New York.

Baker, D. N., J. B. Blake, R. W. Klebesadel, and P. R. Higbie (1986), Highly relativistic electrons in the Earth's outer magnetosphere: 1. Lifetimes and temporal history 1979–1984, *J. Geophys. Res.*, *91*, 4265.

Baker, D. N., J. B. Blake, L. B. Callis, J. R. Cummings, D. Hovestadt, S. Kanekal, B. Blecker, R. A. Mewaldt, and R. D. Zwickl (1994), Relativistic electron acceleration and decay timescales in the inner and outer radiation belts: SAMPEX, *Geophys. Res. Lett.*, *21*, 409.

Baker, D. N., et al. (1997), Recurrent geomagnetic storms and relativistic electron enhancements in the outer magnetosphere: ISTP coordinated measurements, *J. Geophys. Res.*, *102*, 14,141.

Baker, D. N., J. H. Allen, S. G. Kanekal, and G. D. Reeves (1998a), Disturbed space environment may have been related to pager satellite failure, *Eos Trans. AGU*, *79*, 477.

Baker, D. N., X. Li, J. B. Blake, and S. G. Kanekal (1998b), Strong electron acceleration in the Earth's magnetosphere, *Adv. Space. Res.*, *21*, 609.

Callis, L. B., M. Natarajan, J. D. Lambeth, and D. N. Baker (1998), Solar atmospheric coupling by electrons (SOLACE): 2. Calculated stratospheric effects of precipitating electrons, *J. Geophys. Res.*, *103*, 28,421.

Carpenter, D. L., and R. R. Anderson (1992), An ISEE/whistler model of equatorial electron density in the magnetosphere, *J. Geophys. Res.*, *97*, 1097.

Elkington, S. R., M. K. Hudson, and A. A. Chan (1999), Acceleration of relativistic electrons via drift resonant interactions with torroidal-mode Pc-5 ULF oscillations, *Geophys. Res. Lett.*, *26*, 3273.

Friedel, R. H. W., G. D. Reeves, and T. Obara (2002), Relativistic electron dynamics in the inner magnetosphere—A review, *J. Atmos. Sol. Terr. Phys.*, *64*, 265.

Glauert, S. A., and R. B. Horne (2005), Calculation of pitch angle and energy diffusion coefficients with the PADIE code, *J. Geophys. Res.*, *110*, A04206, doi:10.1029/2004JA010851.

Hayakawa, M., M. Parrot, and F. Lefeuvre (1986), The wave normals of ELF hiss emissions observed onboard GEOS 1 at the equatorial and off-equatorial regions of the plasmasphere, *J. Geophys. Res.*, *91*, 7989.

Horne, R. B. (1989), Path-integrated growth of electrostatic waves: The generation of terrestrial myriametric radiation, *J. Geophys. Res.*, *94*, 8895.

Horne, R. B. (2002), The contribution of wave particle interactions to electron loss and acceleration in the Earth's radiation belts during geomagnetic storms, in *Review of Radio Science 1999–2002*, edited by W. R. Stone, pp. 801–828, chap. 33, John Wiley, Hoboken, N. J.

Horne, R. B., and R. M. Thorne (2003), Relativistic electron acceleration and precipitation during resonant interactions with whistler mode chorus, *Geophys. Res. Lett.*, *30*(10), 1527, doi:10.1029/2003GL016973.

Horne, R. B., S. A. Glauert, and R. M. Thorne (2003), Resonant diffusion of radiation belt electrons by whistler mode chorus, *Geophys. Res. Lett.*, *30*(9), 1493, doi:10.1029/2003GL016963.

Horne, R. B., N. P. Meredith, S. A. Glauert, A. Varotsou, R. M. Thorne, Y. Y. Shprits, and R. R. Anderson (2006), Mechanisms for the acceleration of radiation belt electrons, in *The Solar Wind: Corotating Streams and Recurrent Geomagnetism*, *Geophys. Monogr. Ser.*, vol. 167, edited by B. T. Tsurutani et al., in press.

Hudson, M. K., S. R. Elkington, J. G. Lyon, V. A. Machenko, I. Roth, M. Temerin, J. B. Blake, M. S. Gussenhoven, and J. R. Wygant (1997), Simulation of radiation belt formation during sudden storm commencements, *J. Geophys. Res.*, *102*, 14,087.

Hudson, M. K., S. R. Elkington, J. G. Lyon, and C. C. Goodrich (2000), Increase in relativistic electron flux in the inner magnetosphere: ULF wave mode structure, *Adv. Space Res.*, *25*, 2327.

Johnson, M. H., and J. Kierein (1992), Combined Release and Radiation Effects Satellite (CRRES): Spacecraft and mission, *J. Spacecr. Rockets*, *29*, 556.

Lastovicka, J. (1996), Effects of geomagnetic storms in the lower ionosphere, middle atmosphere and troposphere, *J. Atmos. Terr. Phys.*, *58*, 831.

Li, X., and M. A. Temerin (2001), The electron radiation belt, *Space Sci. Rev.*, *95*, 569.

Li, X., I. Roth, M. Temerin, J. Wygant, M. K. Hudson, and J. B. Blake (1993), Simulation of prompt energization, and transport of radiation belt particles during the March 23, 1991 SSC, *Geophys. Res. Lett.*, *20*, 2423.

Li, X., D. N. Baker, M. Temerin, T. E. Cayton, G. D. Reeves, R. A. Christiansen, J. B. Blake, M. D. Looper, R. Nakamura, and S. G. Kanekal (1997), Multi-satellite observations of the outer zone electron variation during the November 3–4, 1993, magnetic storm, *J. Geophys. Res.*, *102*, 14,123.

Liu, W. W., G. Rostoker, and D. N. Baker (1999), Internal acceleration of relativistic electrons by large amplitude ULF pulsations, *J. Geophys. Res.*, *104*, 17,391.

Lyons, L. R., R. M. Thorne, and C. F. Kennel (1972), Pitch-angle diffusion of radiation belt electrons within the plasmasphere, *J. Geophys. Res.*, *77*, 3455.

Meredith, N. P., R. B. Horne, and R. R. Anderson (2001), Substorm dependence of chorus amplitudes: Implications for the acceleration of electrons to relativistic energies, *J. Geophys. Res.*, *106*, 13,165.

Meredith, N. P., R. B. Horne, R. H. A. Iles, R. M. Thorne, R. R. Anderson, and D. Heynderickx (2002a), Outer zone relativistic electron acceleration associated with substorm enhanced whistler mode chorus, *J. Geophys. Res.*, *107*(A7), 1144, doi:10.1029/2001JA900146.

Meredith, N. P., R. B. Horne, D. Summers, R. M. Thorne, R. H. A. Iles, D. Heynderickx, and R. R. Anderson (2002b), Evidence for acceleration of outer zone electrons to relativistic energies by whistler mode chorus, *Ann. Geophys.*, *20*, 967.

Meredith, N. P., R. B. Horne, R. M. Thorne, and R. R. Anderson (2003a), Favored regions for chorus-driven electron acceleration to relativistic energies in the Earth's outer radiation belt, *Geophys. Res. Lett.*, *30*(16), 1871, doi:10.1029/2003GL017698.

Meredith, N. P., M. Cain, R. B. Horne, R. M. Thorne, D. Summers, and R. R. Anderson (2003b), Evidence for chorus driven electron acceleration to relativistic energies from a survey of geomagnetically disturbed periods, *J. Geophys. Res.*, *108*(A6), 1248, doi:10.1029/2002JA009764.

Meredith, N. P., R. M. Thorne, R. B. Horne, D. Summers, B. J. Fraser, and R. R. Anderson (2003c), Statistical analysis of relativistic electron energies for cyclotron resonance with EMIC waves observed on CRRES, *J. Geophys. Res.*, *108*(A6), 1250, doi:10.1029/2002JA009700.

Meredith, N. P., R. B. Horne, R. M. Thorne, D. Summers, and R. R. Anderson (2004), Substorm dependence of plasmaspheric hiss, *J. Geophys. Res.*, *109*, A06209, doi:10.1029/2004JA010387.

Miyoshi, Y., A. Morioka, T. Obara, H. Misawa, T. Nagai, and Y. Kasahara (2003), Rebuilding process of the outer radiation belt during the November 3, 1993, magnetic storm: NOAA and EXOS-D observations, *J. Geophys. Res.*, *108*(A1), 1004, doi:10.1029/2001JA007542.

Obara, T., T. Nagatsuma, M. Den, Y. Miyoshi, and A. Morioka (2000), Main phase creation of ''seed'' electrons in the outer radiation belt, *Earth Planets Space*, *52*, 41.

O'Brien, T. P., K. R. Lorentzen, I. R. Mann, N. P. Meredith, J. B. Blake, J. F. Fennel, M. D. Looper, D. K. Milling, and R. R. Anderson (2003), Energization of relativistic electrons in the presence of ULF power and MeV microbursts: Evidence for dual ULF and VLF acceleration, *J. Geophys. Res.*, *108*(A3), 1329, doi:10.1029/2002JA009784.

O'Brien, T. P., M. D. Looper, and J. B. Blake (2004), Quantification of relativistic electron microbursts losses during the GEM storms, *Geophys. Res. Lett.*, *31*, L04802, doi:10.1029/2003GL018621.

Paulikas, G. A., and J. B. Blake (1979), Effects of the solar wind on magnetospheric dynamics: Energetic electrons at synchronous orbit, in *Quantitative Modeling of Magnetospheric Processes*, *Geophys. Monogr. Ser.*, vol. 21, edited by W. P. Olsen, p. 180, AGU, Washington D. C.

Parrot, M., and F. Lefeuvre (1986), Statistical study of the propagation characteristics of ELF hiss observed on GEOS-1, inside and outside the plasmasphere, *Ann. Geophys.*, *4*, 363.

Reeves, G. D., R. H. W. Friedel, R. D. Belian, M. M. Meiet, M. G. Henderson, T. Onsager, H. J. Singer, D. N. Baker, X. Li, and J. B. Blake (1998), The relativistic electron response at geosynchronous orbit during the January 1997 magnetic storm, *J. Geophys. Res.*, *103*, 17,559.

Santolik, O., M. Parrot, L. R. O. Storey, J. S. Pickett, and D. A. Gurnett (2001), Propagation analysis of plasmaspheric hiss using Polar PWI measurements, *Geophys. Res. Lett.*, *28*, 1127.

Seki, K., Y. Miyoshi, D. Summers, and N. P. Meredith (2005), Comparative study of outer-zone relativistic electrons observed by Akebono and CRRES, *J. Geophys. Res.*, *110*, A02203, doi:10.1029/2004JA010655.

Sheeley, B. W., M. B. Moldwin, H. K. Rassoul, and R. R. Anderson (2001), An empirical plasmasphere and trough density model: CRRES observations, *J. Geophys. Res.*, *106*, 25,631.

Smith, E. J., A. M. Frandsen, B. T. Tsurutani, R. M. Thorne, and K. W. Chan (1974), Plasmaspheric hiss intensity variations during magnetic storms, *J. Geophys. Res.*, *79*, 2507.

Summers, D. (2005), Quasi-linear diffusion coefficients for field-aligned electromagnetic waves with application to the magnetosphere, *J. Geophys. Res.*, *110*, A08213, doi:10.1029/2005JA011159.

Summers, D., and R. M. Thorne (2003), Relativistic electron pitch-angle scattering by electromagnetic ion cyclotron waves during geomagnetic storms, *J. Geophys. Res.*, *108*(A4), 1143, doi:10.1029/2002JA009489.

Summers, D., R. M. Thorne, and F. Xiao (1998), Relativistic theory of wave-particle resonant diffusion with application to electron acceleration in the magnetosphere, *J. Geophys. Res.*, *103*, 20,487.

Summers, D., C. Ma, and T. Mukai (2004), Competition between acceleration and loss mechanisms of relativistic electrons during geomagnetic storms, *J. Geophys. Res.*, *109*, A04221, doi:10.1029/2004JA010437.

Summers, D., R. L. Mace, and M. A. Hellberg (2005), Pitch-angle scattering rates in planetary magnetospheres, *J. Plasma Phys.*, *71*, 237.

Thorne, R. M. (1980), The importance of energetic particle precipitation on the chemical composition of the middle atmosphere, *Pure Appl. Geophys.*, *118*, 128.

Thorne, R. M., E. J. Smith, R. K. Burton, and R. E. Holzer (1973), Plasmaspheric hiss, *J. Geophys. Res.*, *78*, 1581.

Thorne, R. M., S. R. Church, W. J. Malloy, and B. T. Tsurutani (1977), The local time variation of ELF emissions during periods of substorm activity, *J. Geophys. Res.*, *82*, 1585.

Thorne, R. M., T. P. O'Brien, Y. Y. Shprits, D. Summers, and R. B. Horne (2005a), Timescale for MeV electron microburst loss during geomagnetic storms, *J. Geophys. Res.*, *110*, A09202, doi:10.1029/2004JA010882.

Thorne, R. M., R. B. Horne, S. A. Glauert, N. P. Meredith, Y. Shprits, D. Summers, and R. R. Anderson (2005b), The influence of wave-particle interactions on relativistic electron dynamics during storms, in *Inner Magnetosphere Interactions: New Perspectives From Imaging*, *Geophys. Monogr. Ser.*, vol. 159, edited by J. Burch, M. Schulz, and H. Spence, p. 101, AGU, Washington, D. C.

Tsurutani, B. T., and E. J. Smith (1977), Two types of magnetospheric ELF chorus and their substorm dependencies, *J. Geophys. Res.*, *82*, 5112.

Vampola, A. L., J. V. Osborn, and B. M. Johnson (1992), CRRES magnetic electron spectrometer, *J. Spacecr. Rockets*, *29*, 592.

Varotsou, A., D. Boscher, S. Bourdarie, R. B. Horne, S. A. Glauert, and N. P. Meredith (2005), Simulation of the outer radiation belt electrons near geosynchronous orbit including both radial diffusion and resonant interaction with whistler mode chorus waves, *Geophys. Res. Lett.*, *32*, L19106, doi:10.1029/2005GL023282.

West, H. I., R. M. Buck, and G. T. Davidson (1981), The dynamics of energetic electrons in the Earth's outer radiation belt during 1968 as observed by the Lawrence Livermore National Laboratory's Spectrometer on Ogo 5, *J. Geophys. Res.*, *86*, 2111.

J. M. Albert, Air Force Research Laboratory/VSBX, 29 Randolph Road, Hanscom Air Force Base, MA 01731-3010, USA. (jay.albert@hanscom.af.mil)

R. R. Anderson, Department of Physics and Astronomy, University of Iowa, Iowa City, Iowa, IA 52242-1479, USA. (roger-r-anderson@uiowa.edu)

S. A. Glauert, R. B. Horne, and N. P. Meredith, British Antarctic Survey, Natural Environment Research Council, Madingley Road, Cambridge, CB3 0ET, UK. (sagl@bas.ac.uk; r.horne@bas.ac.uk; nmer@bas.ac.uk)

D. Summers, Department of Mathematics and Statistics, Memorial University of Newfoundland, St John's, Newfoundland, Canada, A1C 5S7. (dsummers@math.mun.ca)

R. M. Thorne, Department of Atmospheric and Oceanic Sciences, University of California, Los Angeles, 405 Hilgard Avenue, Los Angeles, CA 90095-1565, USA. (rmt@atmos.ucla.edu)